

Influence of anthocyanin co-pigment on electron transport and performance in black rice dye-sensitized solar cell

Eka Cahya Prima^{1,2,3} · Mariya Al Qibtiya¹ · Brian Yulianto¹ · Suyatman¹ · Hermawan Kresno Dipojono²

Received: 13 December 2015 / Revised: 8 February 2016 / Accepted: 13 February 2016 / Published online: 10 March 2016
© Springer-Verlag Berlin Heidelberg 2016

Abstract This work reports the novel contribution of chlorophyll *b* as natural anthocyanin co-pigment in unpurified black rice extract for improved electron transport and performance of natural dye-sensitized solar cell. The dyes are extracted as prominent photosensitizers by considering the concentration, the dye electronic structure, the extraction, and immersion time. The anthocyanin dye containing 1.92 mM cyanidin-3-O-glucoside structure has been extracted without purification. Interestingly, 0.33 mM chlorophyll *b* is found as a natural co-sensitizer in unpurified anthocyanin. The role of chlorophyll *b* supporting the electron transfer of anthocyanin dye will be investigated for improved cell performance. Both purified and unpurified dyes are compared in the same anthocyanin concentration. The combined Tauc plot and voltametric method will be conducted to show the interfacial electronic band edges of TiO₂-dye-electrolyte. Electrochemical impedance spectroscopy method will investigate electron transfer dynamic in both cell systems. As a result, chlorophyll *b* has dominantly acted as two intermediate states in boosting electron injection and dye regeneration to improve cell efficiency from

1.31 to 2.17 % due to the narrower LUMO–TiO₂ conduction band gap and the narrower HOMO-iodide (I^-) potential gap, respectively. According to the electron transport, the co-sensitizer contributes to the smaller transport resistance ($R_t = 21.9 \Omega$), the higher chemical diffusion coefficient ($D_n = 1.696 \times 10^{-3} \text{ cm}^2/\text{s}$), the higher chemical capacitance ($C_\mu = 14.32 \mu\text{F}$), and the faster electron transport ($\tau_d = 39.88 \mu\text{s}$).

Keywords Dye-sensitized solar cells · Electron transport · Anthocyanin · Chlorophyll *b* · Co-pigment

Introduction

Natural dye-sensitized solar cell (NDSSC) is an attractive solar cell based on the sensitization of natural dyes obtained from the natural resources such as anthocyanin, chlorophyll, betalain, and carotenoid [1]. The materials can be used as a future solar cell candidate due to the abundant, non-toxic, low in cost, and renewable [2]. The dyes absorbing light spectrum are attached onto porous material in order to broaden semiconductor film absorbance. According to the electron transfer dynamic aspects, the dye's lowest unoccupied molecular orbital (LUMO) should be positioned above the conduction band (CB) edge of a semiconductor [3]. After dyes inject the excited electrons, oxidized dyes will be refreshed by iodide ion (I^-) to convert the incident light into electron excitations again. The narrower gap of dyes' LUMO-CB gap compared to the dye's LUMO-triiodide (I_3^-) potential gap will affect to the faster electron injection onto TiO₂ surface compared to the electron recombination captured by triiodide (I_3^-) [4]. Moreover, the higher dyes absorb photons and the more dyes are attached onto TiO₂ film, the more electrons inject through TiO₂ conduction band. Therefore, these parameters should be

✉ Brian Yulianto
brian@tf.itb.ac.id

¹ Advanced Functional Materials Laboratory, Department of Engineering Physics, Institut Teknologi Bandung (ITB), Jalan Ganesha No. 10, Bandung 40132, Jawa Barat, Indonesia

² Computational Material Design and Quantum Engineering Laboratory Department of Engineering Physics, Institut Teknologi Bandung, Jalan Ganesha No. 10, Bandung 40132, Jawa Barat, Indonesia

³ Science Laboratory, Department of Science Education, Universitas Pendidikan Indonesia, Jalan Dr. Setiabudhi No. 229, Bandung 40154, Jawa Barat, Indonesia

considered to improve the performance of natural dye-sensitized solar cell.

Anthocyanin becomes an interesting topic as a natural dye resource for a natural photosensitizer development. The pigment contains hydroxyl groups (–OH) facilitating good dyes' attachment. Moreover, the aromatic ring such as benzopyrone and catechol moieties will support the intermolecular electron transfer through dye skeleton from donor to acceptor group [3]. In nature, this red–purple plant pigment occurs in all higher plants coloring flowers, wines, fruits, stems, leaves, and roots [4]. Black rice is the potential material containing 95 % cyanidin-3-O-glucoside that can be used as a photosensitizer for the natural dye-sensitized solar cell [5]. This dye pigment has been investigated previously by Yulianto [6], Hao [7], Yuliza [8], Saehana [9], and Buraidah [10]. However, the highest black rice based NDSSC efficiency conducted by Hao and co-worker is still 0.32 % [7]. The research optimizing the concentration of anthocyanin based dye achieving 1.42 % efficiency has been investigated by Chien and Hsu at 2 mM dye's concentration [11]. On the other hand, Adhyaksa claimed three main strategies to enhance cell efficiency such as employing of Ag NPs, utilizing TiO₂ nanosheets, and improving the attachment between graminoids and metal nanoparticles employing ligand tethering. In addition, the TiO₂ nanosheet photoelectrode was immersed for 4 days [12]. Therefore, this research will apply two strategies in order to improve the cell performance using two following strategies: utilizing the optimized dye concentration and extending TiO₂ photoelectrode immersion into dye solution.

A natural dye purification is an issue considered to improve the performance of natural photosensitizer. The previous study employed by Gómez-Ortiz shows that the achioté seed purification successfully improved the Bixin absorptivity [13]. Zhou reports the purification of mangosteen pericarp achieving 1.17 % efficiency [14]. Tadesse also reported the purification of *Syzygium guineense* achieving 0.51 % efficiency [15]. The treatment implicitly reports that the extraction solvents play a significant role in the band edge shift of dye. Moreover, the natural dye combination has been conducted by Prima [2], Adhyaksa [12], Furukawa [16], Chang [17], Kumara [18], and Park [19] resulting the dye synergetic effect and the dye absorptivity improvement. Otherwise, Chien reports that the purified natural dye has not directly improved cell efficiency [11]. Therefore, the reports can be viewed that the purified as well as unpurified treatments of natural dyes in terms of photosensitizers are still debatable so that small quantities of co-pigments presented in unpurified dye have to be further investigated as an important aspect influencing dye excitations during the photosensitization process. Both synergetic effects and quenching process compete to either increase or decrease dye's light harvesting efficiency dominantly depending on the electronic structures between two dyes [2, 12]. Hence, the research will investigate the role of natural co-

pigment of unpurified anthocyanin extracted from black rice, which naturally affects to the cell performance.

Chlorophyll is a well-known pigment used by green plants, algae, and bacteria. In nature, chlorophyll is commonly produced in the twin forms such as chlorophylls a-b and chlorophylls c₁-c₂ for green plants and seaweed, respectively [20, 21]. In NDSSC, the main efficient electron injection from the chlorophyll to titanium dioxide is related to the two characteristic π - π^* absorption regions, the weaker Q_y band (550–700 nm) and the intense Soret band in the near UV region (400–450 nm) [12, 22]. The twin pigments are utilized by plants for the fluorescence quenching in the reactions between photosystem (PS) I and II. Some researchers have employed the process for the intermolecular electron transfer as well conducted by Wang [21], Chang [10], and Yu [23]. The research implied that the synergetic effect between two pigments should happen more dominantly than the quenching factor reducing the electron injection to TiO₂. Interestingly, the chlorophyll can also be found as a minor pigment in an anthocyanin pigment. The previous research performed by Calogero et al. investigated pure anthocyanin dye for NDSSC with removing a chlorophyll fraction without considering its pigment effect [24]. It is found that the chlorophyll b in the light harvesting complex II boosts an electron transfer instead of a dye's absorbance improvement analyzed by Förster resonance energy transfer [25, 26].

The Soret band and Q band of chlorophyll b are found at the 465 and 652 nm, respectively. This dye has highly fascinated molar extinction coefficient of 39,350 M⁻¹cm⁻¹ at 652 nm [27]. The Q_y band, which is related to the lowest singlet state excitation, will be red-shifted and strongly broadened due to the interaction with the polar TiO₂ surface [28, 29]. Kay and Graetzel confirmed that 96 % light absorption happens in the Q_y band, and only 25 % incident red photons yield the electron flowing in the external circuit [22, 28]. An electron is rapidly transferred from the excited reaction center of chlorophyll to lower energy acceptor because of the donor state overlap of excited sensitizer with the acceptor states of TiO₂ [29]. The essential π radical cation formation of a Mg containing porphyrin is a central in photo-oxidation [22]. The recombination of injected electrons with oxidized dye molecules will occur due to the cation radical absorption at 720 nm commonly parallels the Q_y band excitation [29]. In contrast, leaving the cation radical process reduced by iodide can decrease the recombination rate and result in a high charge-separation yield [29]. In accordance with the relationship between Soret and Q band and about the injections in the TiO₂, the lower value of intensity ratio is, $I_{\text{soret}}/I_{\text{Qy}}$, the higher Q_y absorption and the greater dye solubility into a specific solvent. The internal conversion of Soret into the Q_y is related to the energy loss reducing DSSC efficiency [22]. The greater Soret energy must be too short-lived to inject electron into TiO₂ efficiently. The higher light harvesting ability respects

to the Q_y wavelength region involved to the electron injection between chlorophyll and TiO_2 film [22]. By understanding the electron injection mechanism in chlorophyll b, this article will investigate the contribution of chlorophyll b as natural co-sensitizer of anthocyanin based unpurified black rice dye with investigating the electron transfer as well as the recombination.

Materials and methods

Natural dye preparations and characterizations

Black rice is obtained from traditional market found in West Java, Indonesia. The dye is extracted at the high molarity from dry black rice by crushing to make powders. The 263-g powders are completely soaked with 380 ml ethanol without the acidic treatment. The solution is stored at the room temperature (25 °C) with dark condition. After 3 weeks, the solution is centrifuged at 4500 rpm for 15 min to filter some aggregates. The solution is subsequently filtered again through 110 mm of Whatman's filter paper using a vacuum pump. Finally, the dye is poured into 50-ml glass bottles and stored in a dark room for an unpurified anthocyanin dye preparation. Furthermore, the purification process of anthocyanin dye follows the previous research conducted by Ordaz-Galindo and Park [5, 30]. The dye extract is dissolved in 15 mL of n-hexane and applied to an Aldrich® calibrated chromatography column with solvent reservoir. The column is eluted with 15 mL of 0.3 % HCl to remove polar constituents and then eluted sequentially with 10:90 (v/v) methanol to water containing 0.3 % HCl, 20:80 (v/v) methanol to water containing 0.3 % HCl, 30:70 (v/v) methanol to water containing 0.3 % HCl, and 40:60 (v/v) methanol to water containing 0.3 % HCl [5]. This isolated anthocyanin extract is used for further study, and it is compared to the unpurified anthocyanin extract. The anthocyanin concentration is measured using Eq. (1), and it is adjusted by diluting the similar solvent [31].

$$\text{Anthocyanin concentration (mM)} = A \cdot DF \cdot 10^3 / \varepsilon \cdot l, \quad (1)$$

Where A is the absorbance, DF is the dilution factor, ε is the molar extinction coefficient, which equals to 26,900 $\text{M}^{-1}\text{cm}^{-1}$, and l is the light-path length (0.1 cm). A is the absorbance given by the Eq. (2)

$$A = (A_{\max} - A_{700})_{\text{pH}1} - (A_{\max} - A_{700})_{\text{pH}4.5} \quad (2)$$

The dye pH of the black rice is adjusted using 0.025 M potassium chloride buffer (pH 1.0) and 0.4 M sodium acetate buffer (pH 4.5). The dye absorbance is measured using Hewlett Packard 8453 Agilent Technologies UV–Vis Spectrophotometer. Moreover, the determination of chlorophyll *b* concentration

follows the method as conducted by Eijkelhoff [32] and Inskeep [27].

In accordance with the empirical equation from Bredas [33], the dye's highest occupied molecular orbital (HOMO) is given by Eq. (3)

$$\alpha h\nu \approx (h\nu - E_g)^n \quad (3)$$

The E_{ox}^{onset} data is plotted from the oxidation potential voltammetry measured by eDAQ potentiostat equipped with e-coder 401; software Echem Ver. 2.1; scan rate 50 mV/s; range of -1600 to $+1600$ mV; initial direction is positive. Three electrodes consisting of a glassy carbon electrode including a platinum counter electrode, and a Ag/AgCl reference electrode in 3 M NaCl solution are used for this measurement using 0.1 M KNO_3 as the supporting electrolyte [34, 35].

The dyes' direct and indirect energy gaps are calculated from UV–Vis spectra data using Tauc Relation as estimated in Eq. (4) [36].

$$E_{HOMO} = -e(E_{ox}^{onset} + 4.4) \quad (4)$$

The dyes' indirect and direct band gaps (E_g) are obtained from the α extrapolation to 0 when $n = 1/2$ and 2, respectively. While E_g is dye's band gap, α is the dye's absorbance, $h\nu$ is the photon energy.

Dye-sensitized solar cell preparations and characterizations

The 2 cm × 2 cm fluorine-doped SnO_2 conductive glass substrate is cleaned using the isopropyl alcohol. Subsequently, the TiO_2 paste (Solaronix, ~13 nm colloidal anatase size and ~120 m^2g^{-1} BET) is deposited onto a glass with the 1.00 × 0.75 cm frame area using doctor blade method resulting ~7.3 μm film thickness. The film is then calcined at 450 °C for 1 h. After that, the film is cooling down to 80 °C, and then, the photoelectrode is immersed in the dye solution for 4 days to ensure that dyes completely attach on the TiO_2 surface. When a cell is fabricated, the dye absorbed- TiO_2 and the sputtered Pt counter electrode is sandwiched and sealed by 50 μm Surlyn ionomer (Dyesol). A drop of standard Γ/I_3^- electrolyte redox containing tetrabutylammonium iodide (0.5 M)/iodine (0.050 M) in acetonitrile solution is inserted into a sandwich cell. In order to improve open circuit voltage due to reducing the recombination rate, additives of 70 mM *tert*-butylpyridine, 0.1 M lithium iodide, and 35 mM pyridine are also applied into the electrolyte adopting the previous research conducted by Adhyaksa and co-workers [12, 37].

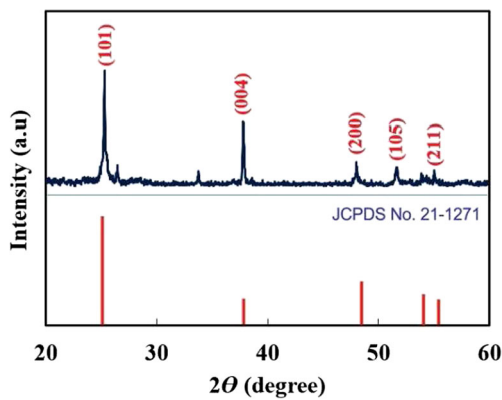


Fig. 1 The X-ray diffraction pattern of TiO₂ nanoparticle compared to the standard TiO₂ anatase of JCPDS No. 21-1271

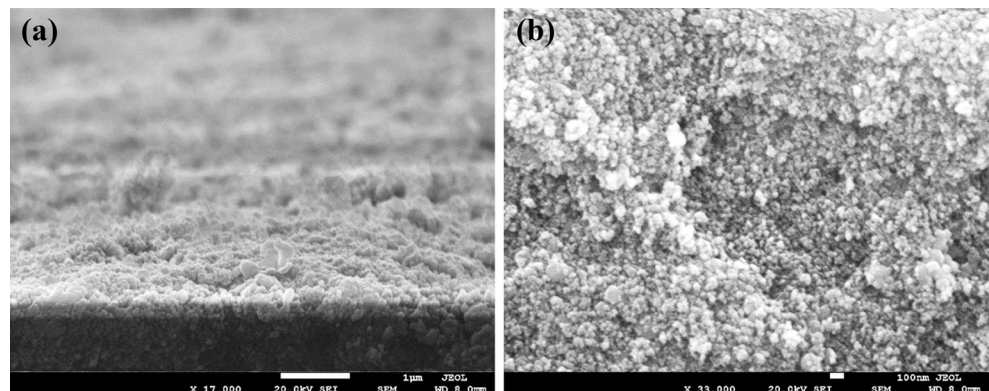
The average TiO₂ grain size is estimated using Scherrer's equation as given in Eq. (5) obtained from X-ray diffraction pattern data measured using the Philips analytical X-ray with Cu radiation.

$$D = \frac{K\lambda}{\beta \cdot \cos\theta} \quad (5)$$

Where K is 0.9 as the factor of dimensionless shape for the spherical particles, λ is 0,154,056 nm, and β is the full width at half-maximum height estimated from the diffraction peaks, and D is the estimated TiO₂ grain size.

The TiO₂ morphologies of both surface and cross-section area are scanned using a scanning electron microscope (JEOL JSM-6360LA). Cell performances are evaluated under AM 1.5 100 mW cm⁻² illumination using standard solar simulator equipped with Keithley 2400 source meter. All characterization measurements are conducted in the ambient temperature. The electrochemical impedance spectroscopy is employed using Agilent Precision LCR Meter E4980A in order to evaluate interfacial charge transfer dynamics of the natural dye. The alternate voltage amplitude is 1.0 mV, and the frequency range is set from 20 Hz to 2 MHz. Finally, the equivalent circuits and impedance parameters are estimated by fitting

Fig. 2 The scanning electron microscope (SEM) images of **a** cross section and **b** surface of TiO₂ nanoparticles



the spectra using Z-View software (v3.3e, Scribner Associate Inc.).

Electron transfer dynamic model

The electron transfer dynamic analysis of the electron injection and the electron recombination is characterized from electrochemical impedance spectroscopy (EIS) data. The analysis method adopts the previous EIS method outstandingly reported by Bisquet [37–42]. The impedance of transmission line for 0 V forward bias potential in dark condition is given in Fig. 6 [37]. The small semicircle curve gives 1/3 transport resistance (R_t) [38].

$$Z = \frac{1}{3}R_t + \frac{R_r}{1 + i\omega/\omega_r} \quad (6)$$

The chemical diffusion coefficient parameter influencing electron injections from dye molecules is analyzed using Eq. (7) [38].

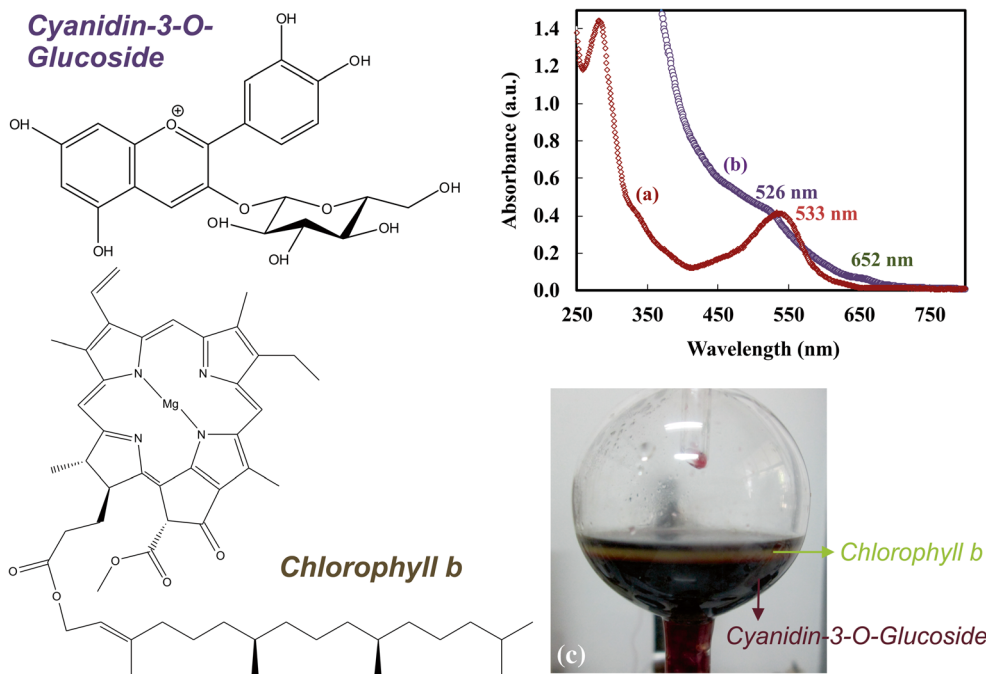
$$D_n = \frac{L_n^2}{\tau_n} = \frac{L^2}{\tau_d} \quad (7)$$

Where L_n is the effective diffusion length, τ_n is the electrons lifetime within the film, L is the film thickness, τ_d is the charge extraction time, and D_n is the chemical diffusion coefficient, the *effective diffusion length* (L_n) can be calculated using Eq. (8) [39, 40].

$$L_n = L\sqrt{\frac{R_r}{R_t}} = L\sqrt{\frac{\tau_n}{\tau_d}} = \sqrt{D_n\tau_n} \quad (8)$$

In a restricted condition, the Warburg impedance will occur in high frequency regimes ($\omega \gg \omega_d$), which show a short straight line in the impedance representation [43]. A large

Fig. 3 The absorption spectra of **a** purified black rice dyes containing cyanidin-3-O-glucoside, **b** unpurified black rice dyes containing cyanidin-3-O-glucoside naturally co-sensitized by chlorophyll b, and figure **c** shows the fractions of cyaniding 3-O-glucoside and chlorophyll b during the chromatography column process.



semicircle of EIS graph in the lower frequency regime indicates the longer electron lifetime and the faster electron transport. The transient time required by electrons to diffuse along L film thickness is given by Eq. (9) [40].

$$\tau_d = R_t C_\mu = \frac{1}{\omega_d} = \frac{L^2}{D_n} \quad (9)$$

The electron recombination commonly occurs due to the electrons recaptured by I_3^- ion [44]. Therefore, the longer electron lifetime will decrease the electron recombination. A good cell performance has the shorter carrier extraction time (τ_d) and the longer electron lifetime time (τ_n). The electron lifetime is given by Eq. (10) [40].

$$\tau_n = R_r C_\mu = \frac{1}{\omega_r} = \frac{L_n^2}{D_n} \quad (10)$$

Results and Discussions

Figure 1 shows the XRD pattern of calcined TiO_2 nanoparticles compared to the anatase standard graph of JCPDS 21-1271. The graph indicates that TiO_2 nanoparticles have a pure anatase phase confirmed by the presence of diffraction peaks at (101), (004), (200), (105), dan (211), which respectively appear at 2θ of 25.30°, 37.78°, 47.98°, 51.58°, and 55.02°. The peaks are similar to the standard peaks of JCPDS 21-1271. Moreover, the TiO_2 nanoparticles do not show the rutile

phase, which usually shows high intensity peaks at 2θ of 27.51°, 36.04°, and 54.23°. According to the grain size calculation corresponding to all planes using Scherrer's equation, the average particle size is approximately 33.9 nm.

Figure 2 shows the surface morphology of TiO_2 nanoparticles characterized using SEM. The film has uniform surface without agglomerations. The pores among nanoparticles facilitate good dye attachment as well as good redox couple (I^-/I_3^-) penetration into the film. Figure 2a shows a flat surface of a TiO_2 film with three dimensional networks of interconnected nanoparticles. It can be considered that the thicker film will increase the amount of dye attachments while the thinner film will boost electron transports, so the film thickness is set to result approximately 7.3 μm film thickness. Figure 2b displays a TiO_2 mesoporous facilitating good dye attachments.

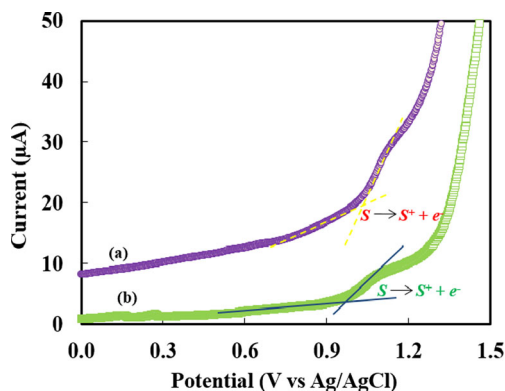


Fig. 4 Voltammetry of black rice dyes at a positive oxidation potential in the dark for **a** cyanidin-3-O-glucoside and **b** chlorophyll b

Table 1 The HOMO-LUMO energy levels and band energy gap energies of dyes

Dye	E_{HOMO} (eV)	E_{LUMO} (eV)	Direct gap (eV)	Indirect gap (eV)
Cyanidin-3-O-glucoside	-5.43	-3.33	2.10	1.72
Chlorophyll <i>b</i>	-5.38	-3.57	1.81	1.69

The uniform TiO_2 adsorptions onto a conductive film reduce dye aggregations.

The UV–Vis graph of purified-unpurified black rice anthocyanin absorbances is depicted in Fig. 3. The purified dye is the same 1.92 mM concentration as unpurified dye. The highly concentrated dye is diluted 20 times using the similar solvent used for extraction process characterized using UV–Vis spectrophotometer resulting in the graph as displayed in Fig. 3. During the purification process, the cyanidin's absorbance peak is red shift from 526 to 533 nm, while the absorbance peak of chlorophyll *b* fraction in the purified dye disappears at 652 nm after dye separation as shown in Fig. 3. The yellowish green and reddish purple colors of fractions indicate chlorophyll *b* and cyanidin-3-O-glucoside dyes, respectively. Interestingly, the purification process increases the anthocyanin absorbance sharpness, but it narrows the overall dye absorbance. Consequently, the narrow absorbance will affect to the decrease of converted photons into dye excitations during photosensitization.

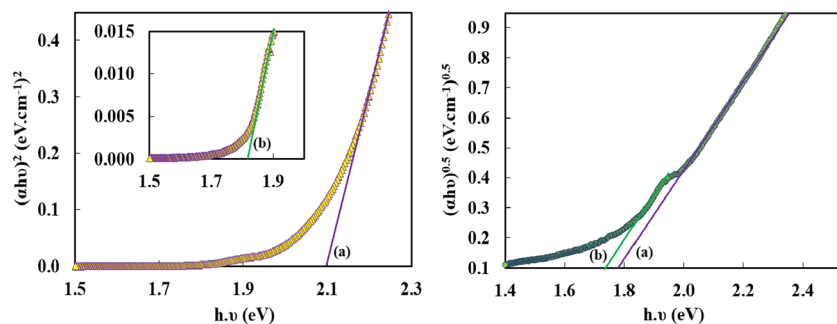
The dye investigation focuses on either the presence or the absence of chlorophyll *b* in anthocyanin dye. The cyanidin structure possessing 8 hydroxyl (–OH) moieties facilitate good dye attachment onto TiO_2 nanoparticles through bidentate and monodentate modes. Moreover, the carbonyl (C=O), hydroxyl (–OH), and carboxylic (–COOH) moieties of chlorophyll *b* also facilitate better dye attachment onto the film. By considering the ratio of cyanidin and chlorophyll *b* which is as much as 6:1, the anthocyanin dye attachment is more dominant than chlorophyll *b*. Nevertheless, the chlorophyll *b* with narrower band gap will be an intermediated state passing through electrons from the excited state of anthocyanin to TiO_2 .

The physical and chemical bindings between anthocyanin and chlorophyll *b* will also happen during dye attachments. The binding interaction will prevent cyanidin desorption because chlorophyll *b* possessing a carboxylic moiety has better

adsorption. The presence of chlorophyll *b* supporting anthocyanin binding will affect to reduce dye- TiO_2 resistance from 24.6 to 21.9 Ω as shown in Table 3. Three aromatic moieties of anthocyanin will delocalize electrons during photosensitization from donor to anchor group. Furthermore, the presence of Mg^{2+} inside chlorophyll *b* as metal center provide the transition character of metal to ligand charge transfer (MLCT) that boosts electron transfers [21, 25]. The electron transfer (τ_d) data of unpurified dye, which is 0.55 μs faster than purified dye as given in Table 3, has supported the phenomenon although the presence of chlorophyll *b* as dye's residue will tend to increase the probability of undesired processes like quenching effect and dyes' intermolecular recombination. The transition character of MLCT will vanish when the anthocyanin dye is purified due to the absence of chlorophyll *b*. The main electronic excitations of both anthocyanin and chlorophyll *b* dyes occur due to the HOMO \rightarrow LUMO transition from bonding orbital (σ) to antibonding (σ^*) resulting in main dye absorbance peak of 526 and 652 nm. Moreover, the intramolecular electron transport also happens through single-double conjugated bonds of cyanidin, porphyrin, and carotenoid skeletons of unpurified dye. The broaden absorbance of unpurified dye along 250 nm through 526 nm will dominantly affect increase of the converted photons into dye excitation and directly improve the short current density of device as tabulated in Table 2.

Figure 4 shows the oxidation onset potentials of cyanidin-3-O-glucoside and chlorophyll *b* extracted from black rice. The onset potentials are then calculated to determine the highest occupied molecular orbital (HOMO) of dyes using empirical Bredas equation as given in Eq. 3 [32]. As a result, the HOMOs of cyanidin and chlorophyll *b* are -5.43 and -5.38 eV, respectively. During the regeneration process, the HOMO position of dye should be more negative than potential of iodide (I^-) ion so that electrons can be captured by oxidized dye [2, 3]. Moreover, the narrower gap between

Fig. 5 Plot of $(\alpha h\nu)^2$ versus $h\nu$ for direct transition and plot of $(\alpha h\nu)^{0.5}$ versus $h\nu$ for indirect transition of black rice dyes containing a cyanidin-3-O-glucoside and b chlorophyll *b*



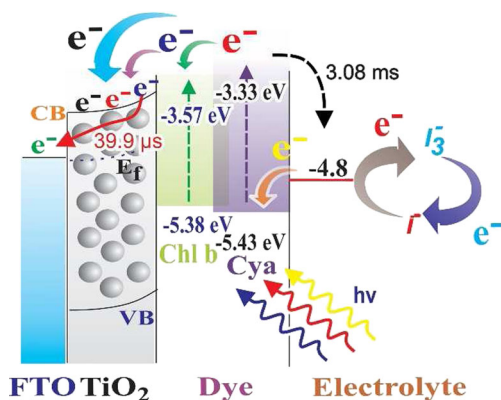


Fig. 6 The natural DSSC structure and its schematic reaction

HOMO of chlorophyll *b* and iodide (*I*⁻) potential will provide better dye regeneration process towards HOMO of anthocyanin dye than the direct regeneration process from iodide to HOMO of cyanidin. Consequently, the chemical capacitance of unpurified dye, which is 1.43 μF higher than the purified dye’s capacitance as shown in Table 3, has proven the reason. On the other hand, it is required that the kinetic of electrons excited from HOMO should be the same as the kinetic of electrons captured from potential redox [40, 41]. Unfortunately, the presence of two states of dyes’ HOMO in unpurified dye will increase the probability of dye’s recombination. Consequently, the electron life time of the unpurified dye is 0.55 ms shorter than the purified dye as shown in Table 3.

Figure 4 shows the direct and indirect band gaps plotted from the Tauc’s graphs. The direct band gap represents the vertical electron transition during the dye excitation, while the indirect band gap includes the change of momentum due to the phonon transfer [47, 48]. Consequently, the indirect band gaps of both dyes is narrower than the direct band gaps due to the longer electron transition as shown in Table 1. Nguyen [47] reported that a direct band gap transition will

dominantly contribute to the electron injection process. Seo [48] also states that the photon energy absorbed by dye will cause phonon emissions when its energy is slightly above the dye’s indirect band gap. The electronic interactions involving all three particles among electrons, photons, and phonons are weaker than a simple electron-photon interaction during a direct band gap transition. Therefore, the direct band gap is then used to determine the vertical transition character of dye during photosensitization. The band gap has been subsequently measured to estimate the dye’s LUMO level following the previous research conducted by Kumara [18]. The electronic structure of unpurified dye contains both anthocyanin and chlorophyll *b*, while the purified dye is only focused on the investigation of cyanidin-3-O-glucoside structure. As shown in Fig. 5a, for direct transition, both cyanidin-3-O-glucoside and chlorophyll *b* show a precise fit resulting in direct band gaps of 2.10 and 1.81 eV, respectively. Then, the indirect band gaps are estimated from the plot of $(\alpha h\nu)^{0.5}$ versus $h\nu$ which yields 1.72 and 1.69 eV for cyanidin-3-O-glucoside and chlorophyll *b*, respectively, as depicted in Fig. 5b.

Table 1 summarizes the HOMO-LUMO levels of dyes obtained from combined voltammetry and Tauc’s plot method. Schematic diagram showing the HOMO and LUMO of black rice dye with the transient time of electron transfer is depicted in Fig. 6. The data shows that cyanidin’s LUMO edge of -3.33 eV is above the chlorophyll *b* LUMO edge of -3.57 eV. In the purified dye, electrons are injected to TiO₂ directly while the LUMO edge of chlorophyll *b* from unpurified dye intermediates electron injection. Consequently, the transient time required by injected electrons from unpurified dye to diffuse along TiO₂ film is faster than direct electron injection from cyanidin through TiO₂ as tabulated in Table 3. Moreover, this phenomenon can happen because the chemical diffusion coefficient of unpurified dye is slightly higher than purified dye.

According to the electron transfer time data as listed in Table 3, the narrower conduction band gap of dye’s LUMO–TiO₂ will boost the intermolecular electron transfer. The effect

Table 2 Photovoltaic parameters of DSSC sensitized by anthocyanin dyes

Dye	DSSC structure	M (mM)	J_{SC} (mA cm ⁻²)	V_{OC} (V)	FF (%)	η (%)	Ref.
Black rice	TiO ₂ -unpurified dye (3 weeks extraction-4 days immersion)-Li/I-Pt	1.92	5.439	0.55	0.74	2.17	-
Black rice	TiO ₂ -purified dye (3 weeks extraction-4 days immersion)-Li/I-Pt	1.92	3.036	0.55	0.63	1.31	-
Black rice	Cu:TiO ₂ -dye (30 min extraction-24 h immersion)-Li/I-Pt	~0.38	0.125	0.12	0.35	0.35	[9]
Black rice	TiO ₂ -Dye (30 min extraction-24 h immersion)-Li/I-Pt	~0.38	0.045	0.45	0.35	0.17	[9]
Black rice	TiO ₂ -dye (5 h extraction-24 h immersion)- (Li/I with chitosan-PEO-NH ₄ I-BMII)-Pt	-	1.213	0.40	0.47	0.23	[10]
Red cabbages	TiO ₂ -dye (10 min extraction with deoxycholic acid coadsorbent-24 h immersion)-Li/I-Pt	2.00	3.470	0.59	0.69	1.42	[11]

Table 3 EIS parameters obtained by fitting the Nyquist plots with the equivalent circuit in Fig. 8c for DSSC based on anthocyanin dyes sensitized TiO₂

Dye	R _t (Ω)	R _r (Ω)	C _μ (μF)	D _n (cm ² /s)	L _n (μm)	τ _d (μs)	τ _n (ms)	η (%)	Ref.
Purified black rice	24.6	281.6	12.89	1.680 × 10 ⁻³	24.70	70.92	3.63	1.31	-
Unpurified black rice	21.9	215.2	14.32	1.696 × 10 ⁻³	22.86	39.88	3.08	2.17	-
Black rice	50.0	4000.0	-	-	-	-	-	0.17	[9]
Cladophora sp.	8.8	222.0	-	8.1 × 10 ⁻⁹	-	-	0.25	0.08	[45]
Mangosteen pericarp	25.4	231.1	-	-	-	-	-	1.17	[14]
Red cabbage	27.6	168.0	8.22	-	-	-	-	0.42	[46]

of combined dye's absorbance and LUMO–CB TiO₂ gap of unpurified dye dominantly results the short current density improvement by 2.403 mA.cm⁻² as shown in Table 2. Unfortunately, the narrower LUMO-triiodide (I₃⁻) gap of unpurified dye will affect the faster electron lifetime where electrons are recaptured by triiodide ion as shown in Table 3.

The typical *J*-*V* curve of purified and unpurified dyes extracted from black rice are shown in Fig. 7. The photovoltaic parameters including short current density (*J*_{sc}), open circuit voltage (*V*_{oc}), fill factor (FF), and power conversion efficiency (η) are tabulated in Table 2. The investigated black rice based DSSC are compared to the previous achievements. The result shows that the unpurified black rice dye with 2.17 % efficiency is superior towards to other previous reports. The photocurrent density, open circuit voltage, fill factor, and overall cell efficiency of unpurified black rice based anthocyanin dye are observed at 5.439 mA cm⁻², 0.55 V, 0.74, and 2.17 %, respectively. Likewise, the photocurrent density, open circuit voltage, fill factor, and overall cell efficiency of purified black rice based anthocyanin dye are observed at 3.036 mA cm⁻², 0.55 V, 0.63, and 1.31 %, respectively. The lower total internal resistance of unpurified dye as listed in Table 3 tends to improve fill factor by 0.11. The unpurified black rice based dyes are compared to the purified black rice based dye in the same anthocyanin concentration of 1.92 mM. The presence of chlorophyll *b* as the minor dye in unpurified black rice extraction

supports the improvement of short current density and overall cell efficiency by 2.403 mA cm⁻² and 0.86 %, respectively.

Compared to the other previous report, it can be analyzed that the longer dye extraction will affect to the higher concentration of extracted dye due to the more pigment molecules released from the anthocyanoplast during the extraction. When the black rice dye is extracted for 30 min, the process has resulted 0.38 mM dye concentration [9]. When the dye is extracted for 3 weeks, the extraction has resulted 1.92 mM of dye concentration. The longer TiO₂ immersion will increase the attached dye onto a photoelectrode. The previous research investigated Cu as metal connector intermediating electron transfer from dye's LUMO through TiO₂ conduction band leading to the cell efficiency improvement at 0.18 % from initial value at 0.17 % to be 0.35 % [9]. On the other hand, the cell performance has been investigated at the presence of chlorophyll *b* as natural co-sensitizer of unpurified black rice dye resulting in the efficiency improvement at 0.86 % from 1.31 to be 2.17 %. Compared to the highly concentrated unpurified red cabbage dyes with 2.00 mM concentration [11], it can be found that the longer dye immersion also improves cell efficiency. The supporting electrolyte of chitosan-PEO-NH₄I-BMII contributes to the cell efficiency improvement [10].

Figure 8 shows the device impedance characteristic using black rice dyes. Figure 8c shows the equivalent circuit element model. The system is simplified due to the restriction of low current conditions, where the electrolyte diffusion impedance (*Z*_d) is vanishingly small. A small arc indicating a high-frequency semicircle is assigned to the charge transport resistance (*R*_t) through TiO₂ nanoparticles. A low-frequency semicircle (A large arc) is ascribed to the dye recombination resistance (*R*_r), and C_μ is the total electrolyte-solid interface capacitance. Moreover, at low frequency with 0 V bias potential, a large arc given by chemical capacitance of the back layer and the charge recombination dominates the impedance [41, 42]. After the excitation, the injected electrons from dye will diffuse through the outer edge of TiO₂ film. Therefore, this condition is assumed as a diffusion-recombination transmission line under reflecting boundary conditions [42].

Table 3 shows the electrochemical impedance data including the transport resistance (*R*_t), the recombination resistance

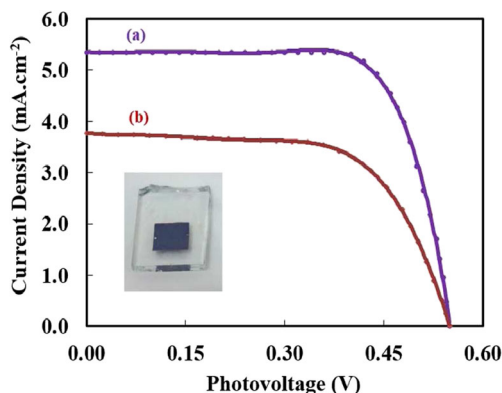


Fig. 7 The *I*-*V* curve of **a** unpurified and **b** purified black rice-based dye-sensitized solar cell. The inset shows the attached dye on the TiO₂ film

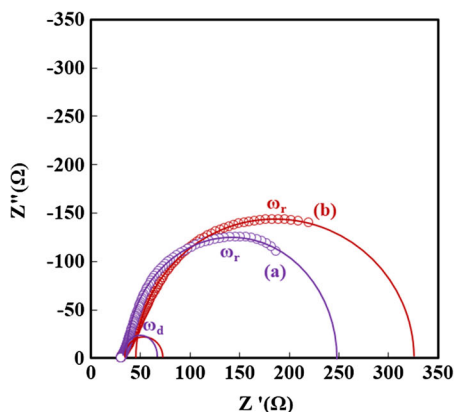
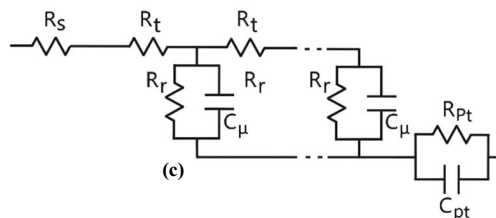


Fig. 8 Nyquist plot of **a** unpurified black rice dye and **b** purified black rice dye at 0 V forward bias potential in dark condition, and **c** shows the equivalent circuit elements showing the diffusion-recombination

(R_t), the chemical diffusion coefficient (D_n), the effective diffusion length (L_n), the charge extraction time (τ_d), and the electron lifetime time (τ_n). The data presents that the transport resistance (R_t) is always shorter than the recombination resistance (R_r). It means that the injected electrons which transport through TiO_2 film are always faster than the recombination. The wider large semicircle resistance (R_r) will affect to reduce the electron recombination [38, 39]. Therefore, the higher recombination resistance of purified dye ($R_r=281.6 \Omega$) compared to the recombination resistance of unpurified dye ($R_r=215.2 \Omega$) has affected to the longer electron lifetime by 0.55 ms. The lower transport resistance of purified dye ($R_t=24.6 \Omega$) compared to the transport resistance of mangosteen pericarp dye ($R_t=25.4 \Omega$) and the higher recombination resistance of purified dye ($R_r=281.6 \Omega$) compared to the recombination resistance of mangosteen pericarp dye ($R_r=231.1 \Omega$) have resulted the superior efficiency of purified dye. Although the transport resistance of *Cladophora* sp. dye is the smallest among all natural dyes, the poor chemical diffusion coefficient ($8.1 \times 10^{-9} \text{ cm}^2/\text{s}$) and the shorter lifetime (0.25 ms) tend to significantly decrease its efficiency excluding considering its dye concentration attached onto the film. Moreover, the smaller transport resistance ($R_t=21.9 \Omega$), the higher chemical diffusion coefficient ($D_n=1.696 \times 10^{-3} \text{ cm}^2/\text{s}$), the higher chemical capacitance ($C_\mu=14.32 \mu\text{F}$), and the faster electron transport ($\tau_d=39.88 \mu\text{s}$) of unpurified anthocyanin dye outstandingly improve the cell performance. It can be analyzed that chlorophyll *b* has dominantly acted as two intermediate states in boosting electron injection and dye regeneration to achieve the superior cell efficiency of 2.17 % due to the narrower LUMO– TiO_2 conduction band gap and the narrower HOMO–iodide (Γ) potential gap, respectively, where unpurified dye is compared to the purified dye in the same concentration of 1.92 mM. Otherwise, the presence of chlorophyll *b* in unpurified dye also reduces electron life time (τ_n) by 0.55 ms as well as effective diffusion length (L_n) by 1.84 μm . The size of chlorophyll *b* molecules attached onto



transmission line under reflecting boundary condition, which is a highly idealized photoanode schematic at various potentials in the dark

TiO_2 film might prevent the adsorption of cyanidin molecules to penetrate through the film.

Conclusions

Chlorophyll *b* as natural co-sensitizer of anthocyanin dye has been investigated including the electron transfer as well as the recombination. The purification process increases the anthocyanin absorbance sharpness, but it narrows the overall dye absorbance. Consequently, the narrow absorbance will affect the decrease of converted photons into dye excitations during photosensitization. The main electronic excitations of both anthocyanin and chlorophyll *b* dyes occurs due to the HOMO \rightarrow LUMO transition from bonding orbital (σ) to antibonding (σ^*) resulting in main dye absorbance peak of 526 and 652 nm. The broaden absorbance of unpurified dye along 250 nm through 526 nm will dominantly affect increase of the converted photons into dye excitation and directly improve the short current density. This finding has investigated the presence of chlorophyll *b* as natural co-sensitizer of unpurified black rice dye resulting in the efficiency improvement from 1.31 to 2.17 %. According to the electron transport, the co-sensitizer contributes to the smaller transport resistance ($R_t=21.9 \Omega$), the higher chemical diffusion coefficient ($D_n=1.696 \times 10^{-3} \text{ cm}^2/\text{s}$), the higher chemical capacitance ($C_\mu=14.32 \mu\text{F}$), and the faster electron transport ($\tau_d=39.88 \mu\text{s}$).

Acknowledgments The research underlying this paper is partially supported by Penelitian Unggulan Perguruan Tinggi (2016) and Penprinas MP3EI (2013–2015), National Innovation System (SINAS) Research Incentive Program Kementerian Riset, Teknologi, dan Pendidikan Tinggi Republik Indonesia (RT-2014-741), KK Research and Innovation Program, Institut Teknologi Bandung (2014), and Ikatan Alumni ITB Research Grant (2014–2015).

References

- Calogero G, Bartolotta A, Di Marco G, Di Carlo A, Bonaccorso F (2015) Vegetable-based dye-sensitized solar cells. *Chem Soc Rev* 44:3244–3294
- Prima EC, Yuliarto B, Suendo V, Suyatman (2014) Improving photochemical properties of *Ipomea pescaprae*, *Imperata cylindrica* (L.) Beauv, and *Paspalum conjugatum* Berg as photosensitizers for dye sensitized solar cells. *J Mater Sci Mater Electron* 25:4603–4611
- Cahya Prima E, Yuliarto B, Kresno Dipojono H (2015) Theoretical investigation of anthocyanidin aglycones as photosensitizers for dye-sensitized TiO₂ solar cells. *Adv Mat Res* 1112:317–320
- Bridle P, Timberlake CF (1997) Anthocyanins as natural food colours—selected aspects. *Food Chem* 58:103–109
- Park YS, Kim SJ, Chang HI (2008) Isolation of anthocyanin from black rice (*Heugjinjubyeo*) and screening of its antioxidant activities. *Korean J Microbiol Biotechnol* 36:55–60
- Yuliarto B, Septina W, Fuadi K, Fanani F, Muliani L, Nugraha (2010) Synthesis of nanoporous TiO₂ and its potential applicability for dye-sensitized solar cell using antocyanine black rice. *Adv Mater Sci Eng*. doi:10.1155/2010/789541
- Hao S, Wu J, Huang Y, Lin J (2006) Natural dyes as photosensitizers for dye-sensitized solar cell. *Sol Energy* 80:209–214
- Yuliza E, Saehana S, Rahman DY, Rosi M, Mikrajuddin A (2013) Enhancement performance of dye-sensitized solar cells from black rice as dye and black ink as counter electrode with inserting copper on the space between TiO₂ particles by using electroplating method. *Mater Sci Forum* 737:85–92
- Saehana S, Yuliza E, Arifin P, Abdullah M (2013) Dye-sensitized solar cells (dssc) from black rice and its performance improvement by depositing interconnected copper (Copper Bridge) into the space between TiO₂ nanoparticles. *Mater Sci Forum* 737:43–53
- Buraidah MH, Teo LP, Yusuf SNF, Noor MM, Kufian MZ, Careem MA (2011) Arof AK (2011) TiO₂/chitosan NH₄I(+I₂)-BMII-based dye-sensitized solar cells with anthocyanin dyes extracted from black rice and red cabbage. *Int J Photoenergy*. doi:10.1155/2011/273683
- Chien CY, Hsu BD (2013) Optimization of the dye sensitized solar cell with anthocyanin as photosensitizer. *Sol Energy* 98:203–211
- Adhyaksa GWP, Prima EC, Lee DK, Ock I, Yatman S, Yuliarto B, Kang JK (2014) A light harvesting antenna using natural extract graminoids coupled with plasmonic metal nanoparticles for biophotovoltaic cells. *Adv Energy Mater* 4:1400470. doi:10.1002/aenm.201400470
- Gómez-Ortíz NM, Maldonado IAV, Espadas ARP, Rejoñ GJM, Barrios JAA, Oskama G (2010) Dye-sensitized solar cells with natural dyes extracted from Achiote seeds. *Sol Energy Mater Sol Cells* 94:40–44
- Zhou H, Wu L, Gao Y, Ma T (2011) Dye-sensitized solar cells using 20 natural dyes as sensitizers. *J Photochem Photobiol, A* 219:188–194
- Tadesse S, Abebe A, Chebude Y, Garcia IV, Yohannes T (2012) Natural dye-sensitized solar cells using pigments extracted from *Syzygium Guineense*. *J Photon Energy* 2:027001–1. doi:10.1117/1.JPE.2.027001
- Furukawa S, Lino H, Iwamoto T, Kukita K, Yamauchi S (2009) Characteristics of dye-sensitized solar cells using natural dye. *Thin Solid Films* 518:526–529
- Chang H, Lo YJ (2010) Pomegranate leaves and mulberry fruit as natural sensitizers for dye-sensitized solar cells. *Sol Energy* 84:1833–1837
- Kumara NTRN, Ekanayake P, Lim A, Liew LYC, Iskandar M, Ming LC, Senadeera GKR (2013) Layered co-sensitization for enhancement of conversion efficiency of natural dye sensitized solar cells. *J Alloys Compd* 581:186–191
- Park KH, Kim TY, Park JY, Jin EM, Yim SH, Fisher JG, Lee JW (2013) Photochemical properties of dye-sensitized solar cell using mixed natural dyes extracted from *Gardenia Jasminoide* Ellis. *J Electroanal Chem* 689:21–25
- Kirchhoff H, Hinz HJ, Rösgen J (2003) Aggregation and fluorescence quenching of chlorophyll a of the light-harvesting complex II from spinach in vitro. *Biochim Biophys Acta* 1606:105–116
- Wang XF, Zhan CH, Maoka T, Wada Y, Koyama Y (2007) Fabrication of dye-sensitized solar cells using chlorophylls c1 and c2 and their oxidized forms and from *Undaria pinnatifida* (Wakame). *Chem Phys Lett* 447:79–85
- Calogero G, Citro I, Crupi C, Di Marco G (2014) Absorption spectra and photovoltaic characterization of chlorophyllins as sensitizers for dye-sensitized solar cells. *Spectrochim Acta A Mol Biomol Spectrosc* 132:477–484
- Yu D, Zhu G, Liu S, Ge B, Huang F (2013) Photocurrent activity of light-harvesting complex II isolated from spinach and its pigments in dye-sensitized TiO₂ solar cell. *Int J Hydro Energy* 38:16740–16748
- Calogero G, Yum JH, Sinopoli A, Di Marco G, Grätzel M, Nazeeruddin MK (2012) Anthocyanins and betalains as light-harvesting pigments for dye-sensitized solar cells. *Sol Energy* 86:1563–1575
- Argyroudi-Akoyunoglou JH, Akoyunoglou G (1970) Photoinduced changes in the chlorophyll a to chlorophyll b ratio in young bean plants. *Plant Physiol* 46:247–249
- Eads DD, Castner EW Jr, Alberte RS, Mets L, Fleming GR (1989) Direct observation of energy transfer in a photosynthetic membrane: chlorophyll b to chlorophyll a transfer in LHC. *J Phys Chem* 93:8271–8275
- Inskeep WP, Bloom PR (1985) Extinction coefficients of chlorophyll a and b in N, N-dimethylformamide and 80% acetone. *Plant Physiol* 77:483–485
- Kay A, Graetzel M (1993) Artificial photosynthesis. 1. Photosensitization of titania solar cells with chlorophyll derivatives and related natural porphyrins. *J Phys Chem* 97:6272–6277
- Kay A, Humphry-Baker R, Graetzel M (1994) Artificial photosynthesis. 2. Investigations on the mechanism of photosensitization of nanocrystalline TiO₂ solar cells by chlorophyll derivatives. *J Phys Chem* 98:952–959
- Ordaz-Galindo A, Wesche-Ebeling P, Wrolstad RE, Rodriguez-Saona L, Argai-Jamet A (1999) Purification and identification of Capulin (*Prunus serotina* Ehrh) anthocyanins. *Food Chem* 65:201–206
- Wrolstad RE, Durst RW, Lee J (2005) Tracking color and pigment changes in anthocyanin products. *Trends Food Sci Tech* 16:423–428
- Eijkelhoff C, Dekker JP (1997) A routine method to determine the chlorophyll a, pheophytin a and β-carotene contents of isolated photosystem II reaction center complexes. *Photosynth Res* 52:69–73
- Bredas JL, Silbey R, Boudreaux DS, Chance RR (1983) Chain-length dependence of electronic and electrochemical properties of conjugated systems: polyacetylene, polyphenylene, polythiophene, and polypyrrole. *J Am Chem Soc* 105:6555–6559
- Lim A, Kumara NTRN, Tan AL, Mirza AH, Chandrakanthi RNL, Petra MI, Ekanayake P (2015) Potential natural sensitizers extracted from the skin of *Canarium odontophyllum* fruits for dye-sensitized solar cells. *Spectrochim Acta A* 138:596–602
- Kumara NTRN, Kooh MRR, Lim A, Petra MI, Voo NY, Lim CM, Ekanayake P (2013) DFT/TDDFT and experimental studies of natural pigments extracted from black tea waste for DSSC application. *Int J Photoenergy*. doi:10.1155/2013/109843
- Tauc J, Grigorovici R, Vancu A (1966) Optical properties and electronic structure of amorphous germanium. *Phys Stat Sol* 15:627–636

37. Wu J, Lan Z, Lin J, Huang M, Huang Y, Fan L, Luo G (2015) Electrolytes in dye-sensitized solar cells. *Chem Rev* 115:2136–2173
38. Bisquert J, Vikhrenko VS (2002) Analysis of the kinetics of ion intercalation. Two state model describing the coupling of solid state ion diffusion and ion binding processes. *Electrochim Acta* 47: 3977–3988
39. Bisquert J (2002) Theory of the impedance of electron diffusion and recombination in a thin layer. *J Phys Chem B* 106:325–333
40. Bisquert J (2004) Chemical diffusion coefficient of electrons in nanostructured semiconductor electrodes and dye-sensitized solar cells. *J Phys Chem B* 108:2323–2332
41. Bisquert J, Compte A (2001) Theory of the electrochemical impedance of anomalous diffusion. *J Electroanal Chem* 499:112–120
42. Bisquert J, Fabregat-Santiago F, Mora-Seró I, Garcia-Belmonte G, Giménez S (2009) Electron lifetime in dye-sensitized solar cells: theory and interpretation of measurements. *J Phys Chem C* 113: 17278–17290
43. Bisquert J, Garcia-Belmonte G, Pitarch Á (2003) An explanation of anomalous diffusion patterns observed in electroactive materials by impedance methods. *ChemPhysChem* 4:287–292
44. Warburg E (1901) Ueber die polarisationscapacität des platins. *Ann Phys* 311:125–135
45. Lim A, Haji Manaf N, Tennakoon K, Chandrakanthi RLN, Lim LBL, Bandara JMR, Ekanayake P (2015) Higher performance of DSSC with dyes from *Cladophora* sp. as mixed cosensitizer through synergistic effect. *J Biophys*. doi:10.1155/2015/510467
46. San Esteban ACM, Enriquez EP (2013) Graphene–anthocyanin mixture as photosensitizer for dye-sensitized solar cell. *Sol Energy* 98:392–399
47. Nguyen VH, Chan HY, Wu JC (2013) Synthesis, characterization and photo-epoxidation performance of Au-loaded photocatalysts. *J Chem Sci* 125:859–867
48. Seo DK, Hoffmann R (1999) Direct and indirect band gap types in one-dimensional conjugated or stacked organic materials. *Theor Chem Acc* 102:23–32